Self-similar flow field of consumer sprays

Hannes Hinterbichler*, Helfried Steiner, Günter Brenn
Institute of Fluid Mechanics and Heat Transfer, Graz University of Technology, Austria
*Corresponding author: hannes.hinterbichler@tugraz.at

Abstract
Self-similar fields are observed in flows when there is no time or length scale imposed. The self-similar behavior of flows allows for a description of the velocity field as a function of one self-similar coordinate only. Further to many single-phase flows, there is evidence for self-similar behavior of both the liquid and the gas phase in spray flows also. In most works on self-similar sprays, the liquid and the gas were injected simultaneously, often resulting in a small slip velocity between the two phases. The dynamics of these sprays can be modeled analogous to single-phase jets, accounting for variable fluid density.
In the present work we experimentally investigate the dynamics of sprays from consumer spray cans for body and textile care in order to predict the transport and drying behaviors of the spray drops. The aim is to assess health risks from nanoparticle-laden sprays. In the sprays investigated, only liquid is ejected into quiescent ambient air, resulting in large slip velocities between the liquid and the gas phase. Hence, solely momentum transfer between the two phases induces the motion of the gas phase. Phase-Doppler measurements reveal the evolution of the spray drop and gas flow fields to be modeled. Three sprays at different liquid Weber and Ohnesorge numbers are considered. We show that, for all the sprays investigated, the gas flow fields exhibit self-similar behavior close to the well-known single-phase jet, but with different axial scaling of the self-similar variables, since the momentum flow rate increases downstream, while it is constant for single-phase jets. In order to model the gas flow we transform the equations of motion from boundary layer theory into a self-similar form, accounting for momentum transfer between the gas and the liquid phases in the flow at constant pressure. The self-similar ansatz introduced yields a self-similar solution for the gas flow fields of the sprays investigated. A priori unknown coefficients of the ansatz are determined with the help of the phase-Doppler data. The self-similar solution obtained for the gas flow field shows excellent agreement with the experimental results.

Keywords
liquid-phase driven flow, self-similarity transform, turbulent momentum transport

Introduction

Sprays are of great importance in many kinds of industrial processes including spray combustion, spray drying and crop spraying in agriculture [1] and thus have a significant influence on many products of everyday life. Recent developments in nanotechnology encourage the potential use of manufactured nanomaterials in consumer sprays, such as hair sprays, antiperspirants and waterproofing sprays in order to enhance the desired effects. The present study focuses on the modeling of the dynamics of such consumer-type sprays in order to finally gain insights on the fate of the nanoparticulate content possibly present.
Flows without imprinted scales may assume self-similar behavior on which the modeling of the dynamics can be built. Self-similar phenomena in sprays were reported in many different studies, for example self-similarity of the mean axial drop velocity in air-assisted atomization [2] and self-similarity of the gas flow field and the evaporation source term in combusting spray flames [3]. Others modeled the spray as a single-phase jet with variable density obtaining similar scaling of the variables as for the round single-phase jet [4, 5, 6]. In these studies liquid and gas were often injected simultaneously with negligible change of the cross sectional average gas and liquid momentum flow rates endorsing self-similar behavior as observed for single-phase jets [7]. In the present work we focus on the self-similar modeling of sprays where the motion of the gas flow is induced by momentum transfer from the liquid phase exclusively, as recently reported in [8].
Our investigation is based on sprays generated with a standard-consumer type nozzle using phase-Doppler anemometry (PDA). Two different liquids are sprayed at three different liquid mass flow rates in the order of magnitude observed for commercially available products. Since only liquid is ejected from the nozzle, the motion of the gas phase is solely induced due to the interaction with the droplets. Propellant gases, which are often used in commercially available spray cans, and their effects on the atomization process, i.e. flash boiling, are not considered in the present study.
We demonstrate that the gas flow fields of the sprays exhibit self-similar behavior, and we derive a self-similar solution of the basic equations of motion from boundary layer theory, analogous to the single-phase round jet [9], but with account for the momentum transfer between the liquid and the gas phase.

Material and methods

We investigate the characteristics of consumer-type sprays experimentally with phase-Doppler anemometry. To generate the sprays, a simple single-phase dispenser with an orifice diameter of approximately $D_{or} = 0.4\,\mathrm{mm}$, where the liquid is ejected with an imposed swirl, is used. We measure velocity components in axial direction, u_l, and radial

Table 1. Parameters of the experiments performed. The fluid properties are taken from [10] at a temperature of 20 °C.

	Spray 1	Spray 2	Spray 3
Liquid mass flow rate $\dot{m}_l$ [g/s]	2.00	2.92	2.45
Location of measurement planes z/D_{or}	38 - 375	38 - 450	38 - 625
Density ρ_l [kg/m^3]	998.2	998.2	981.7
Dynamic viscosity μ_l [mPa s]	1.00	1.00	1.40
Surface tension against air σ [mN/m]	72.8	72.8	51.3
Weber number *We*	1395	2974	2921
Ohnesorge number *Oh*	0.0059	0.0059	0.0099

direction, v_l, as well as the diameter d of 100,000 drops at each measurement point. The sprays generated are considered as axially symmetric. A detailed description of the experimental setup can be found elsewhere [8]. All experiments were carried out at temperatures of 20 ± 1 °C.
Three sprays at different liquid mass flow rates are considered. For spray 1 ($\dot{m}_l = 2.00\,\mathrm{g/s}$) and spray 2 ($\dot{m}_l = 2.92\,\mathrm{g/s}$) water is used as the test liquid, whereas the liquid of spray 3 ($\dot{m}_l = 2.45\,\mathrm{g/s}$) is an aqueous ethanol solution with an ethanol content of 10 mass percent. The atomization process is governed by two non-dimensional numbers, namely Weber and Ohnesorge number, which are calculated as

$$We = \frac{\rho_l D_{or} \bar{u}_{or}^2}{\sigma} \qquad \text{and} \qquad Oh = \frac{\mu_l}{\sqrt{\rho_l\, \sigma D_{or}}} \tag{1}$$

respectively. $\bar{u}_{or}$ is the mean axial bulk velocity of the liquid phase at the nozzle exit calculated from the liquid mass flow rate $\dot{m}_l$. Spray 1 and 2 differ in Weber number, whereas spray 3 has a larger Ohnesorge number than the first two sprays and approximately the same Weber number as spray 2. Experimental parameters, fluid properties and the non-dimensional numbers calculated according to (1) are listed in table 1.

Experimental results

In this section the experimentally obtained liquid and gas flow fields are presented and discussed. The experimental data of spray 1 and 2 corresponds to the results reported in [8].

Velocity of the liquid flow field

In figure 1, the mean axial drop velocity $\bar{u}_l$ is plotted as a function of radial and axial coordinate. For spray 1 (left) bell-shaped profiles with a maximum at the spray axis can be observed. Spray 2 (center) shows a local minimum and a peak farther radially outwards in the mean axial drop velocity profile closest to the nozzle exit ($z = 15\,\mathrm{mm}$). Farther downstream a second peak arises along the spray axis. The shapes of the profiles obtained for spray 3 are between those of the first two sprays. The difference between the mean axial drop velocity profiles of the sprays may be attributed to the state of flow and the geometry of the nozzle. Due to the swirl induced by the inner geometry of the nozzle, a hollow conical sheet is formed at high liquid flow rates, resulting in fine atomization, while at low flow rates the spray obtained may rather be in the so-called tulip stage, leading to coarser atomization [1]. This explanation is supported by the obtained drop size distributions (not shown), where a shift to larger drop sizes can be observed for spray 1 compared to sprays 2 and 3.

Velocity of the gas flow field

The velocity of the gas flow field is derived from drops with very low Stokes numbers. These are typically the smallest drops, which act as nearly massless tracer particles due to their low relaxation time. In the present case drops

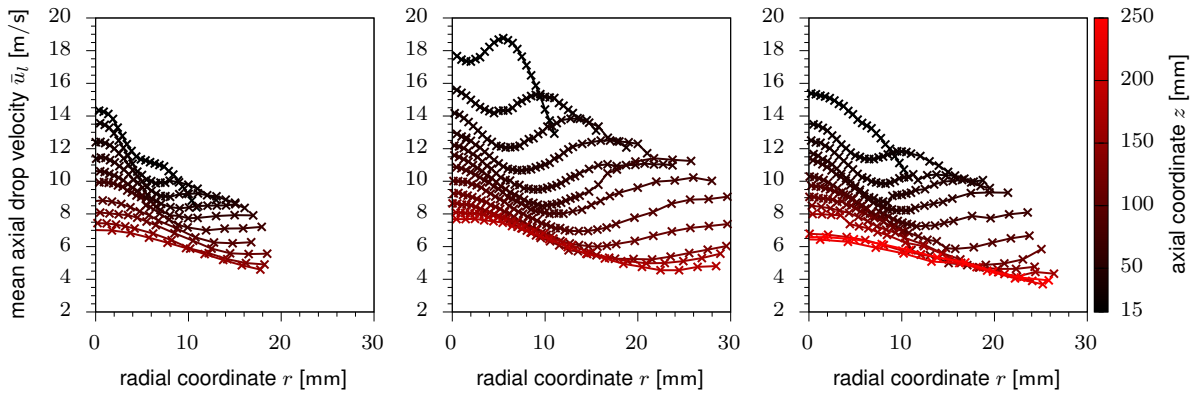

Figure 1. Experimentally obtained mean axial drop velocities. Left: spray 1. Center: spray 2. Right: spray 3.

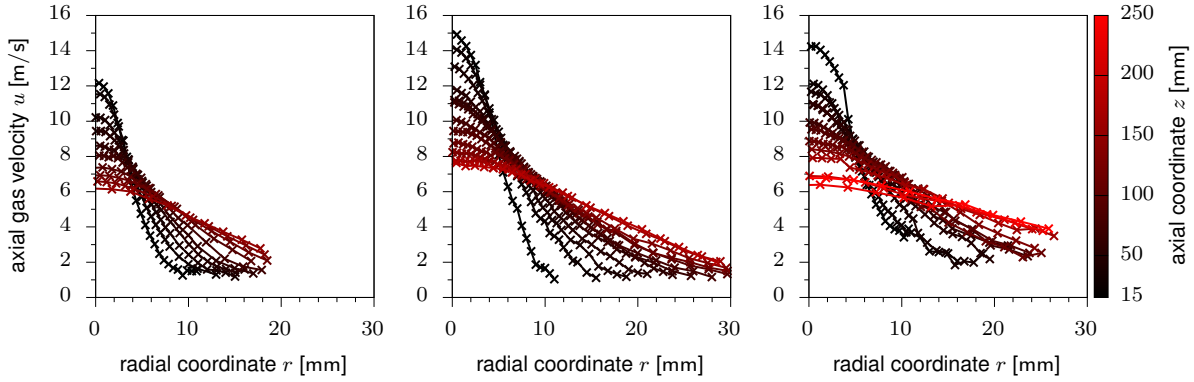

Figure 2. Axial velocity of the gas flow field of the sprays deduced from the mean velocity of small drops. Left: spray 1. Center: spray 2. Right: spray 3.

with $d < 15\,\mu\text{m}$ are considered to determine the mean gas velocity. A detailed description of the procedure for the calculation the gas flow field from PDA data for these types of spray is given elsewhere [8].
In figure 2, the axial velocity profiles of the gas phase are shown. For all three sprays, the profiles are bell-shaped, with a maximum at the spray axis. Downstream, a decrease of the gas velocity along the spray axis and a radial expansion of the velocity profiles can be observed.

Self-similarity of the gas flow field
In the present section we derive a self-similar solution for the gas flow fields of the consumer-type sprays investigated. The deduction of unknown model coefficients from the experimental PDA data is demonstrated.

Equations of motion
For the analytical description, the gas flow fields of the sprays are considered as turbulent boundary layer-type flow. The corresponding axis-symmetric boundary layer equations, with zero pressure gradient in axial direction and Boussinesq eddy viscosity concept applied to compute the turbulent shear stress, are given in cylindrical coordinates as

$$\frac{\partial u}{\partial z} + \frac{1}{r}\frac{\partial (vr)}{\partial r} = 0 \qquad \text{continuity} \tag{2}$$

$$u\frac{\partial u}{\partial z} + v\frac{\partial u}{\partial r} = \nu_t \frac{1}{r}\frac{\partial}{\partial r}\left(r\frac{\partial u}{\partial r}\right) + f_d \qquad z\text{-momentum} \tag{3}$$

The contribution of the viscous shear stress is neglected since we expect that $\nu_t \gg \nu$. Here ν_t denotes the turbulent eddy viscosity which is assumed to be approximately constant in the present case, analogously to the self-similar description of turbulent single-phase jets. The momentum source term f_d is introduced into the z-momentum equation in order to account for the exchange of momentum between the liquid and the gas phase. As reported in [8], our ansatz for a self-similar solution reads

$$\eta = D\frac{r}{(z-z_0)^{\alpha}}, \qquad \Psi = C(z-z_0)f(\eta), \qquad f_d = C^2D^4(z-z_0)^{1-4\alpha}\Omega(\eta) \tag{4}$$

and is chosen such that, after introduction into equation (3), an ordinary differential equation (ODE) for $f(\eta)$, independent of z, is obtained. η represents the self-similar coordinate, $f(\eta)$ is the self-similar shape function which depends on η only and Ψ denotes the Stokesian stream function, which inherently satisfies continuity (2) and allows for calculation of the axial and radial velocity components as follows

$$u = \frac{1}{r}\frac{\partial \Psi}{\partial r}, \qquad v = -\frac{1}{r}\frac{\partial \Psi}{\partial z} \tag{5}$$

The two constants C and D are introduced for dimensional reasons, z_0 denotes the virtual origin of the flow field and α is an exponent. $\Omega(\eta)$ is the self-similar shape function of the momentum source term, depending on η only. The transform of the z-momentum equation (3) in self-similar coordinate reads

$$(1-2\alpha)f'^2 - \eta f\left(\frac{f'}{\eta}\right)' = \frac{\nu_t}{C}\eta\left[\eta\left(\frac{f'}{\eta}\right)'\right]' + \eta^2\Omega(\eta) \tag{6}$$

It is important to note that for $\alpha = 1$ and $\Omega(\eta) = 0$ this equation reduces to the well-known self-similar momentum equation for the round single-phase jet [9]. The axial and radial velocity components are calculated from (5) as

$$u = CD^2(z-z_0)^{1-2\alpha}\frac{f'}{\eta} \qquad \text{and} \qquad v = CD(z-z_0)^{-\alpha}\left(\alpha f' - \frac{f}{\eta}\right), \tag{7}$$

respectively. From the boundary conditions for the velocity components, the following boundary conditions for the self-similar shape function $f(\eta)$ can be deduced

$$u|_{r\to 0} = \text{finite} \qquad \Rightarrow f'(0) = 0 \tag{8}$$

$$v|_{r\to 0} = 0 \qquad \Rightarrow f(0) = 0 \tag{9}$$

$$v|_{r\to \infty} = 0 \qquad \Rightarrow f'(\infty) = 0 \tag{10}$$

In order to obtain a solution for the self-similar shape function $f(\eta)$ from (6), the parameters C, D, z_0 and α as well as the turbulent eddy viscosity ν_t and the shape function of the source term $\Omega(\eta)$ have to be determined.

Determination of the parameters introduced by the ansatz for self-similarity

To determine the four constants in the ansatz for self-similarity (4), we relate the self-similar transformed flow quantities to our experimental data. First, we match the experimental velocity data on the symmetry axis $u_0(z)$, where $r = 0$, i.e. $\eta = 0$, with the expression obtained from equation (7) for the axial velocity at the spray axis

$$u_0 = \underbrace{CD^2 f''(0)}_{U_{exp}} (z - z_0)^{1-2\alpha}, \tag{11}$$

where U_{exp} denotes the constant product of C, D^2 and $f''(0)$. Second, as required by self-similarity, we enforce the experimentally measured normalized gas velocities u/u_0 to satisfy

$$\frac{u}{u_0} = \text{constant} \qquad \text{for} \qquad \eta = D\frac{r}{(z - z_0)^{\alpha}} = \text{constant} \tag{12}$$

As a third constraint, the self-similar solution has to meet the axial dependency of the momentum flow rate $\mathcal{I}(z)$ of the gas phase, which is defined as

$$\mathcal{I} = 2\pi\rho \int_{r=0}^{\infty} u^2 r \,\mathrm{d}r = \underbrace{2\pi\rho C^2 D^2 \int_{\eta=0}^{\infty} \frac{f'^2}{\eta}\,\mathrm{d}\eta}_{M_{exp}} (z - z_0)^{2-2\alpha} \tag{13}$$

M_{exp} denotes the constant product of the indicated quantities. In order to determine the experimental momentum flow rate, a continuous analytical representation of the experimentally obtained values u at discrete positions r_i (see figure 2) is required. Thus, we fit the experimental axial velocity profiles of every cross section to a bell-shaped function which reads

$$u(r) = \frac{A_1}{(1 + A_2 r^2)^2}, \tag{14}$$

where A_1 and A_2 are independent fit parameters. The obtained velocity profiles are in excellent agreement with the experimental data (not shown).

Using the three constraints given by equations (11), (12) and (13) we obtain the parameters α and z_0 from fits to experimental data. Moreover we get the constant products of parameters denoted U_{exp} and M_{exp}, as well as the ratios of η/D associated with the normalized gas velocities u/u_0 (see equation (12)). The obtained values are listed in table 2 along with values for ν_t calculated from PDA data. The procedure to determine ν_t is shown in the next section of this work.

The exponent α is almost constant for all three cases with a value close to approximately $2/3$. The values for the virtual origins are slightly negative, indicating locations inside the nozzle. The two fit parameters U_{exp} and M_{exp} which relate to the self-similar solution via

$$U_{exp} = CD^2 f''(0) \qquad \text{and} \qquad M_{exp} = 2\pi\rho C^2 D^2 \int_{\eta=0}^{\infty} \frac{f'^2}{\eta}\,\mathrm{d}\eta, \tag{15}$$

respectively, represent two constraints for the determination of the constants C and D.

Table 2. Parameters determined from (11) - (13). $\nu = 0.154\,\mathrm{mm^2/s}$ and denotes the kinematic viscosity of air at 20 °C.

	Spray 1	Spray 2	Spray 3
α	0.66	0.71	0.65
z_0 [mm]	-2.2	-14.8	-3.1
U_{exp} [$\mathrm{m^{2\alpha}/s}$]	3.50	3.73	4.45
M_{exp} [$\mathrm{kg\,m^{2\alpha-1}/s^2}$]	0.12	0.19	0.31
ν_t [Pa s]	80ν	100ν	110ν

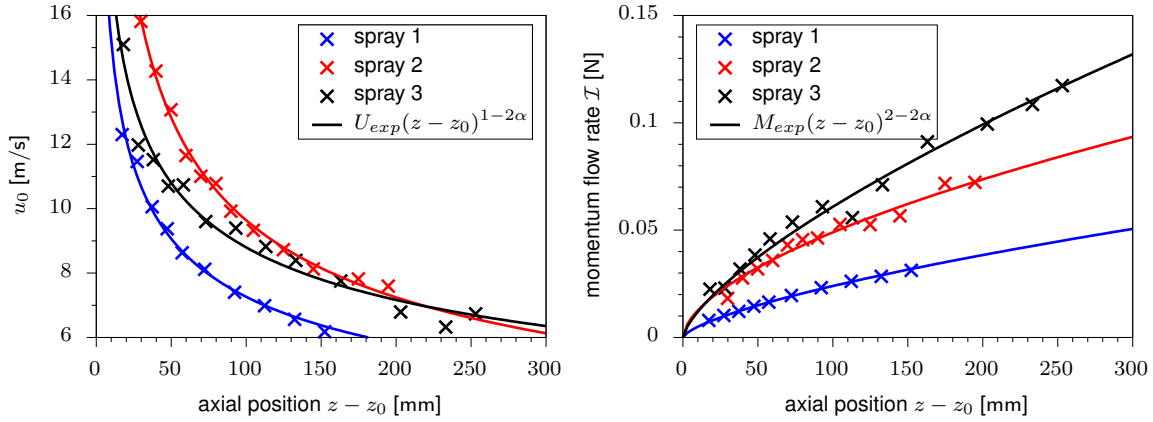

Figure 3. Left: Decrease of the axial gas velocity along the symmetry axis of the spray. Right: Increase of the momentum flow rate of the gas phase with its axial position in the spray. The parameters used for computing the curves in both diagrams are listed in table 2.

To verify that the obtained parameters match the experimental data, in figure 3, on the left-hand side, the decrease of the axial gas velocity along the spray axis and on the right-hand side, the increase of the axial gaseous momentum flow rate is shown for all three sprays. For the latter, the symbols correspond to the experimental data calculated from (13) with (14). The solid lines are fit curves of the equations (11) (left) and (13) (right). Excellent agreement can be observed.
In figure 4, the scaled velocity profiles u/u_0 are plotted against the self-similar coordinate η/D for the three sprays. In all cases they collapse very well to a single profile. Minor deviations can be observed for the profiles closest to the nozzle exit ($z = 15\,\mathrm{mm}$; black symbols). This may be attributed to the fact that in this region of the sprays the self-similar behavior is not fully developed yet, a well-known phenomenon also observed for the single-phase jet.

Turbulent eddy viscosity

The turbulent eddy viscosity ν_t is estimated with the help of the Boussinesq eddy viscosity concept by

$$-\overline{u'v'} = \nu_t \frac{\partial u}{\partial r}, \tag{16}$$

where u' and v' are the axial and radial velocity fluctuations of the gas phase. The cross correlation of the velocity fluctuations $\overline{u'v'}$ is calculated from PDA data considering only the smallest droplets $d < 15\,\mu\mathrm{m}$, which are assumed to represent the gas flow field. The equation to determine $\overline{u'v'}$ from PDA data reads

$$\overline{u'v'} = \frac{\sum_i \sum_j n_{ij}(u-u_i)(v-v_j)}{\sum_i \sum_j n_{ij}}, \tag{17}$$

where n_{ij} is the number of drops with the radial velocity v_j in the axial velocity class u_i. In figure 5, the profiles of $\overline{u'v'}$ are plotted against the self-similar coordinate in the cross section $z = 25\,\mathrm{mm}$ for the three sprays. The solid lines represent the product of the radial gradient of the axial gas velocity, calculated from (14) multiplied with a constant eddy viscosity ν_t. We conclude that the earlier assumption of a constant eddy viscosity for the whole flow field (other cross sections not shown) is reasonably well justified. The obtained values for ν_t are listed in table 2 and are two

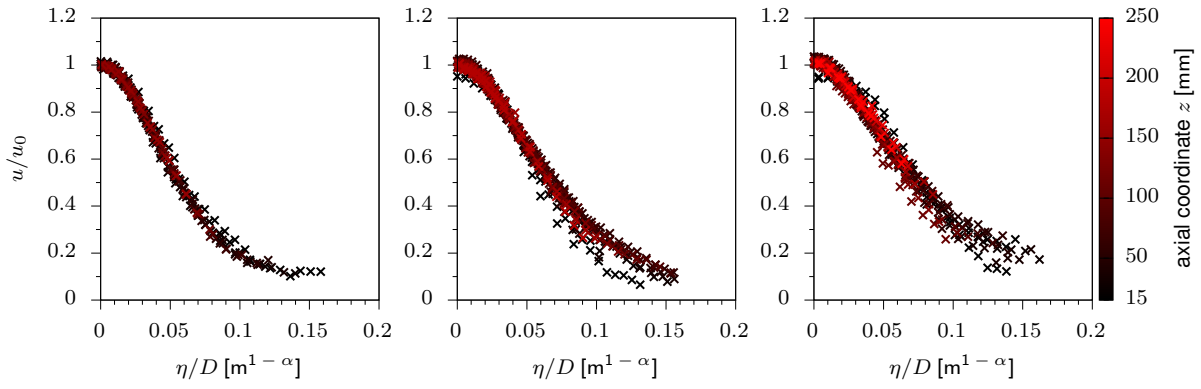

Figure 4. Self-similar profiles of the gas flow field. Left: spray 1. Center: spray 2. Right: spray 3.

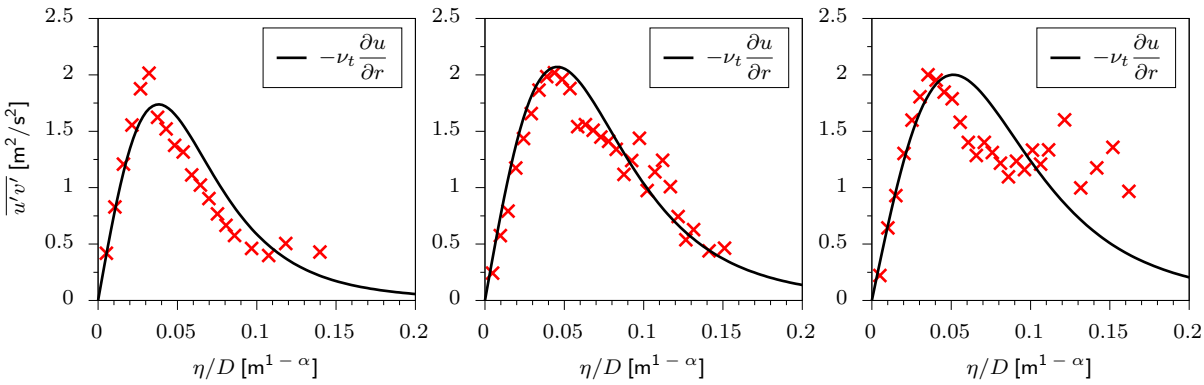

Figure 5. Radial profiles of the cross correlations of the turbulent fluctuations at $z = 25\,\mathrm{mm}$. Left: spray 1. Center: spray 2. Right: spray 3.

orders of magnitude larger than the molecular kinematic viscosity of air ν, in a similar range as the values obtained by others for the single phase jet [11, 12].

Self-similar solution

To obtain a solution for the self-similar shape function $f(\eta)$ from equation (6), two different approaches may be considered. On the one hand, one could provide an approximate shape function of the momentum source term $\Omega(\eta)$, assume a value for the constant C and solve equation (6) numerically. The obtained solution must satisfy the two conditions given by equation (15).

On the other hand, one could postulate a solution for $f(\eta)$ which satisfies the boundary conditions (8) to (10) and represents the self-similar velocity profiles shown in figure 4. If $f(\eta)$ then also satisfies the conditions given by equation (15) it may be introduced into the transformed z-momentum equation (6) to determine the shape of the momentum source term. We will follow the latter approach since it immediately allows for an analytical expression for both $f(\eta)$ and $\Omega(\eta)$.

We define the self-similar shape function $f(\eta)$ as

$$f(\eta) = \frac{\eta^2}{1 + \frac{1}{4}\eta^2}, \tag{18}$$

similar to the solution of the round single-phase jet [9]. Using (18), the constants C and D can immediately be calculated from (15) to

$$C = \frac{3}{8\pi\rho}\frac{M_{exp}}{U_{exp}} \qquad \text{and} \qquad D = 2\sqrt{\frac{\pi\rho}{3}}\frac{U_{exp}}{\sqrt{M_{exp}}} \tag{19}$$

With knowledge of the constant D for all three sprays, the scaled velocities profiles given in figure 4 can be unified in a single diagram as given in figure 6. The self-similar axial velocity profiles of all three sprays collapse very well to a single curve. The self-similar velocity profile obtained with (18) from equation (7) yields

$$\frac{u}{u_0} = \frac{f'}{\eta f''(0)} = \frac{1}{\left(1 + \frac{1}{4}\eta^2\right)^2} \tag{20}$$

and is represented in figure 6 by the solid green line. The agreement between model and experimental data is excellent.

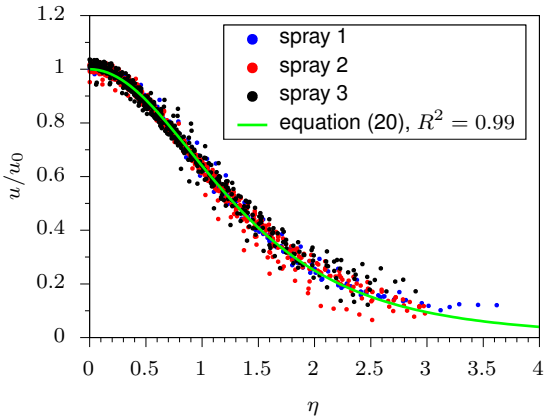

Figure 6. Unified self-similar axial velocity profile of the gas flow field.

Momentum source term

Flux terms in sprays cannot be measured directly with phase-Doppler anemometry, but their computation is a straightforward process. However, results obtained may differ up to an order of magnitude from their real values as for example reported by [13, 14]. This can be attributed to the problem of accurately calculating the effective sampling area in PDA measurements which depends, among other things, on droplet diameter, droplet trajectory and probe volume measurement errors [14]. Thus, we do not attempt to extract an exact functional description of the momentum source term $\Omega(\eta)$ from our PDA data, but only an estimate of its approximate shape.

We assume that the loss of axial momentum flux of the liquid phase is balanced by the radial redistribution of liquid mass (and therefore momentum) and the momentum transferred to the gas phase. The balance reads

$$\frac{\partial}{\partial z}\left(\Phi(r,z)\right) + \frac{\rho_l}{r}\frac{\partial}{\partial r}\left(r\sum_i \bar{u}_i(r,z)\,\phi_i(r,z)\right) = -\rho f_d(r,z), \tag{21}$$

where $\Phi(r,z)$ is the axial liquid momentum flux, $\phi_i(r,z)$ the radial liquid volume flux and $\bar{u}_i(r,z)$ the mean axial drop velocity in drop size class i. From equation (21) we calculate the radial profiles of f_d in every spray cross section, scale them with the axial dependency of the momentum source term prerequired for self-similarity $(z-z_0)^{1-4\alpha}$, see equation (4), and compute the radial mean of the obtained profiles resulting in an estimation for the self-similar shape function of the momentum source term $\Omega(\eta)$.

The results are plotted in figure 7 on the left-hand side against the self-similar coordinate η (dashed lines). For spray 1 the profile is approximately bell shaped with a maximum at the spray axis, whereas for sprays 2 and 3 a local minimum in the profile can be seen at the spray axis with a peak farther radially outwards. These results agree with the mean axial drop velocities observed in figure 1, where for spray 1 (left) the majority of the liquid mass is assumed to be at the spray axis and for sprays 2 and 3 a peak in the velocity profiles arises radially outwards due to the formation of a hollow conical liquid sheet. Note that all three profiles estimated from PDA data are scaled for reasons explained at the beginning of this section in order to obtain an order of magnitude of unity.

With knowledge of the solution (18) of the self-similar shape function, the analytical expression for the shape of the momentum source term can be directly expressed from equation (6) as

$$\Omega(\eta) = \frac{2}{\left(1+\frac{1}{4}\eta^2\right)^4}\left[2-4\alpha+\eta^2+\frac{\nu_t}{C}(2-\eta^2)\right] \tag{22}$$

The corresponding results are shown in figure 7 on the left-hand side (solid lines). Radially outwards (large values of η) the obtained profiles agree with the experimental estimates of $\Omega(\eta)$ (dashed lines). As we approach the spray axis ($r=0$, i.e. $\eta=0$) the curves deviate. Especially for sprays 2 and 3, we obtain negative values for the momentum source term, indicating that momentum is transferred from the gas to liquid phase. This is, however, not expected since only liquid is ejected into quiescent ambient air, resulting in large slip velocities. We attribute this discrepancy to the underestimation of the turbulent eddy viscosity by our experimental PDA data, which is deduced from the cross correlation of the turbulent velocity fluctuations $\overline{u'v'}$ of small drops $d < 15\,\mu\text{m}$. Note that, for statistical reasons, the smallest drop size class is $0\,\mu\text{m} < d < 5\,\mu\text{m}$. As shown by [15], drops or particles in turbulent flow may follow velocity fluctuations in a turbulent flow field only up to turbulent frequencies depending on particle size and density, and on fluid properties of the ambient phase. We presume that, due to the statistical classification of the drops in our sprays into drop size classes, we capture large turbulent structures up to a certain frequency in the turbulent energy spectrum and obtain results in the correct order of magnitude for $\overline{u'v'}$, i.e. ν_t. However, high-frequency turbulent phenomena are missed and therefore ν_t is underestimated. This assumption is supported by comparing relaxation time scales of the drops and the gas phase (not shown). Note, that others used “glycerin smoke” [16, p. 40] with drop diameters of approximately only $1\,\mu\text{m}$ in order to measure the turbulent fluctuations in the single-phase round jet [16].

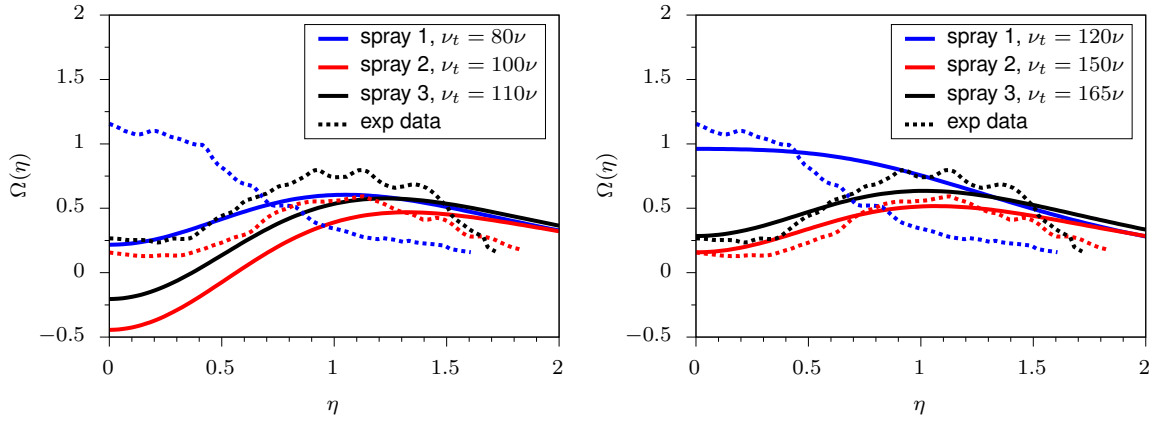

Figure 7. Shape functions of the momentum source terms estimated from PDA data (dashed lines) and calculated by equation (22) (solid lines).

An increase of the values obtained for ν_t listed in table 2 by $50\,\%$ results in profiles for the momentum source term which can be seen in figure 7 on the right-hand side. The theoretical predictions calculated by (22) now match the experimental estimates reasonably well.

Summary and conclusions

Sprays generated by a consumer-type spray can were investigated experimentally with PDA at three different pairs of Weber and Ohnesorge number. We introduce a similarity ansatz based on the equations of motion for boundary layer-type flows to model the gas flow field of the sprays, similar to a round single-phase jet but with account for momentum transfer from the liquid to the gas phase. We show a procedure to determine all parameters of the model, like the constants of the ansatz, the turbulent eddy viscosity and the momentum source term with the help of our PDA data. Most notably, we obtain a self-similar shape function similar to the one obtained for the round single-phase jet, but with significantly different scaling of the self-similar variables. The obtained self-similar solution is in excellent agreement with the experimental results.

Acknowledgments

The authors gratefully acknowledge the financial support from the Austrian Research Promotion Agency FFG (project no. 849876). This work is supported by SIINN ERA-NET, funded under the ERA-NET scheme of the Seventh Framework Programme of the European Commission, Research Directorate - General, Grant Agreement No. 265799.

Nomenclature

Latin symbols

A_1	fit parameter [m/s]
A_2	fit parameter [$1/\mathrm{m}^2$]
C	constant [m^2/s]
d	drop diameter [m]
D	constant [$\mathrm{m}^{\alpha\,-\,1}$]
D_{or}	orifice diameter [m]
$f(\eta)$	self-similar shape function
f_d	momentum source term [m/s^2]
$\mathcal{I}$	axial momentum flow rate [N]
$\dot{m}$	mass flow rate [kg/s]
M_{exp}	fit parameter [$\mathrm{kg\,m}^{2\alpha\,-\,1}/\mathrm{s}^2$]
Oh	Ohnesorge number
r	radial coordinate [m]
R^2	coefficient of determination
u, v	axial and radial velocity component [m/s]
u', v'	axial and radial velocity fluctuation [m/s]
U_{exp}	fit parameter [$\mathrm{m}^{2\alpha}/\mathrm{s}$]
We	Weber number
z	axial coordinate [m]
z_0	virtual origin [m]

Greek symbols

α	exponent
η	self-similar coordinate
μ	dynamic viscosity [Pa s]
ν	kinematic viscosity [m^2/s]
ν_t	eddy viscosity [m^2/s]
ρ	density [kg/m^3]
σ	surface tension [N/m]
ϕ	radial liquid volume flux [$\mathrm{m}^3/(\mathrm{m}^2\,\mathrm{s})$]
Φ	axial liquid momentum flux [N/m^2]
Ψ	Stokesian stream function [m^3/s]
$\Omega(\eta)$	self-similar shape function of the momentum source term

Subscripts

i, j	size or velocity class
l	liquid phase, drop
or	orifice

References

[1] Lefebvre, A. H., and McDonell, V. G., 2017, Atomization and Sprays. Taylor & Francis, Boca Raton.
[2] Li, X., and Shen J., 1999, *Journal of Propulsion and Power*, 15, pp. 103-110.
[3] Karpetis, A. N., and Gomez A., 1999, *Journal of Fluid Mechanics*, 397, pp. 231-258.
[4] Shearer, A. J., Tamura, H., and Faeth G. M., 1979, *Journal of Energy*, 3, pp. 271-278.
[5] Faeth G. M., 1983, *Progress in Energy and Combustion Science*, 9, pp. 1-76.
[6] Panchagnula, M. V., and Sojka P. E., 1999, *Fuel*, 78, pp. 729-741.
[7] George, W. K., 1989, Advances in Turbulence (George and Arndt, eds), pp. 39-73, Hemisphere, New York.
[8] Hinterbichler, H., Steiner, H., and Brenn, G., 14th International Conference on Liquid Atomization and Spray Systems, July 22-26, 2018, Chicago, IL, USA.
[9] Schlichting, H., 1933, *Zeitschrift für Angewandte Mathematik und Mechanik*, 13 (4), pp. 260-263.
[10] Khattab, I. S., Bandarkar, F., Fakhree, M. A. A, and Jouyban, A., 2012, *Korean Journal of Chemical Engineering*, 29 (6), pp. 812-817.
[11] Lumely, J. L., and Tennekes, H., 1972, A first course in turbulence. MIT Press, Cambridge.
[12] Peters, N., ERCOFTAC Summer School, September 15-19, 1997, Aachen, Germany.
[13] Bade, K. M., and Schick, R. J., 2011, *Atomization and Sprays*, 21 (7), pp. 537-551.
[14] Sipperley, C. M., Bade, K. M., and Schick, R. J., 14th International Conference on Liquid Atomization and Spray Systems, July 22-26, 2018, Chicago, IL, USA.
[15] Chao, B. T, 1964, *Österreichisches Ingenieur-Archiv*, 18, pp. 7-21.
[16] Hussein, H. J, Capp, S. P., and George, W. K., 1994, *Journal of Fluid Mechanics*, 258, pp. 31-75.